Durability and physical characterization of anti-fogging solution for 3D-printed clear masks and face shields

Succhay Gadhar [Equal first author, 1], **Shaina Chechang** [Equal first author, 1], **Philip Sales** [1], **Praveen Arany** [Corresp. 1]

[1] Oral Biology, Biomedical Engineering, and Surgery, University at Buffalo, Buffalo, NY, USA

Corresponding Author: Praveen Arany
Email address: praveenarany@gmail.com

Background. The COVID-19 pandemic brought forth the crucial roles of personal protective equipment (PPE) such as face masks and shields. Additive manufacturing with 3D printing enabled customization and generation of transparent PPEs. However, these devices were prone to condensation from normal breathing. This study was motivated to seek a safe, non-toxic, and durable anti-fogging solution. **Methods**. We used additive 3D printing to generate the testing apparatus for contact angle, sliding angle, and surface contact testing. We examined several formulations of carnauba wax to beeswax in different solvents and spray-coated them on PETG transparent sheets for testing contact and sliding angle, and transmittance . Further, the integrity of this surface following several disinfection methods such as soap, Isopropyl Alcohol, or water alone with gauze, paper towels, and microfiber, along with disinfectant wipes, was assessed. **Results**. The results indicate a 1 : 2 ratio of carnauba to beeswax in Acetone optimally generated a highly hydrophobic surface (contact angle 150.3 + 2.1 ° and sliding angle 13.7 + 2.1 °) with maximal transmittance. The use of soap for disinfection resulted in the complete removal of the anti-fogging coating, while Isopropyl Alcohol and gauze optimally maintained the integrity of the coated surface. Finally, the contact surface testing apparatus generated a light touch (5000 N/m^2) that demonstrated good integrity of the antifogging surface. **Conclusions**: This study demonstrates that a simple natural wax hydrophobic formulation can serve as a safe, non-toxic, and sustainable anti-fogging coating for clear PPEs compared to several commercial solutions.

Durability and Physical Characterization of Anti-Fogging Solution for 3D-Printed Clear Masks and Face Shields

Succhay Gadhar[1,*], Shaina Chechang[1,*], Philip Sales[1], Praveen R. Arany[1,$]

[1] Oral Biology, Biomedical Engineering and Surgery, University at Buffalo, NY, USA

[*] *Equal contributions*

[$]**Address correspondence to:**

Praveen R. Arany B.D.S., M.D.S., M.M.Sc., Ph.D.

3435 Main Street, BRB 553,

Buffalo, NY 14214.

E-mail: prarany@buffalo.edu

Phone: 716-829-3479

Keywords: Face shields, Masks, Anti-fogging

ABSTRACT

Background. The COVID-19 pandemic brought forth the crucial roles of personal protective equipment (PPE) such as face masks and shields. Additive manufacturing with 3D printing enabled customization and generation of transparent PPEs. However, these devices were prone to condensation from normal breathing. This study was motivated to seek a safe, non-toxic, and durable anti-fogging solution.

Methods. We used additive 3D printing to generate the testing apparatus for contact angle, sliding angle, and surface contact testing. We examined several formulations of carnauba wax to beeswax in different solvents and spray-coated them on PETG transparent sheets for testing contact and sliding angle, and transmittance. Further, the integrity of this surface following several disinfection methods such as soap, Isopropyl Alcohol, or water alone with gauze, paper towels, and microfiber, along with disinfectant wipes, was assessed.

Results. The results indicate a 1 : 2 ratio of carnauba to beeswax in Acetone optimally generated a highly hydrophobic surface (contact angle 150.3 $\pm$ 2.1 ° and sliding angle 13.7 $\pm$ 2.1 °) with maximal transmittance. The use of soap for disinfection resulted in the complete removal of the anti-fogging coating, while Isopropyl Alcohol and gauze optimally maintained the integrity of the coated surface. Finally, the contact surface testing apparatus generated a light touch (5000 N/m^2) that demonstrated good integrity of the antifogging surface.

Conclusions: This study demonstrates that a simple natural wax hydrophobic formulation can serve as a safe, non-toxic, and sustainable anti-fogging coating for clear PPEs compared to several commercial solutions.

INTRODUCTION

The COVID-19 pandemic has had a significant toll on the public health, biomedical, and financial aspects that have significantly changed society.(1,2) Among various healthcare services, the presence of SARS-CoV in the nasal and upper respiratory tract presented significant challenges for dentists and anesthetists. Clinical dentistry presented a significant challenge due to the proximity and inherent aerosol-generating procedures.(3-5) The use of personal protection equipment (PPE) such as face masks and face shields was integral in reducing the spread of infections among the general population. (6) While dentistry routinely utilizes face masks, double masking, and the highly protective N95, the shielding nature and the lack of face-to face exposure further compounded the pandemic fear and anxiety in patients naturally apprehensive about their dental visits. (7-9) Another major limitation of these masks is that they hinder effective communication due to the lack of non-verbal cues such as facial expressions and lips movements. (10-12) This is particularly challenging in patients with differently-abled hearing due to increased signal-to-noise from the ambient noise in dental operatories. (13-16) The use of transparent masks and face shields has been demonstrated to improve these limitations. (17)

Another major challenge during the early phase of the pandemic was the significant disruption of the PPE supply chain requiring local innovations where additive manufacturing using 3D printing came to the forefront. (18-21) The ability to generate required quantities based on need and additional customization for individual applications were significant advantages of this approach. (22) Building on this, in collaboration with e-NABLE, a 3D printing community, students at the University at Buffalo School of Dental Medicine generated transparent PPEs using 3D printing and vacuum casting. Among them, several custom designs were specifically generated to accommodate commercially available dental loupes that are made available freely online.(23) These clear masks and face shields were well accepted and generated much enthusiasm among clinical users. Besides dentistry, another group of clinicians that notably adopted these clear PPEs were the local speech and hearing-impaired clinics. However, an immediate limitation of this approach reported by users was the fogging due to the moisture from regular breathing. This essentially negated the advantage of the transparent nature of these masks and face shields and presented additional hindrance of needing repetitive wipe-downs.

The commercially available anti-fogging solutions used for eyeglasses and car exteriors contain polydimethylsiloxane and silica nanoparticles.(24) The long-term use of these solutions was considered unsuitable due to their potential for skin irritation, and potential inhalation or ingestion. Hence, we sought to identify a non-toxic, antifogging coating for the transparent masks and face shields for long-term use. To design such a solution, specific design criteria needed to be met. The surface of a water droplet is attracted to the bulk of the droplet due to cohesion which results in their beading. The shape that a drop takes on a given surface depends on the surface tension of the fluid and the physical characteristics of the surface. A surface-fluid interface is the contact angle that measures the wettability of a surface. Contact angles can vary from hydrophilic (less than or equal to 30°) to hydrophobic (greater than or equal to120°), where the higher the contact angle, the lower its wettability. (25) Another measure of the extent of moisture retention on a surface is the sliding angle which is measured by tilting the surface with the solution bead to determine the angle at which it rolls off. The more hydrophobic the surface, the higher the angle of loss of fluid droplets.(26) Another key design aspect of the anti-fogging solution would be its resistance to wear due to repeated skin surface contact during mask use. The ideal solution would offer a thin, durable coating for daily use that would not need repetitive applications while maintaining maximal transparency.

Natural products offer attractive non-toxic coatings. Prior studies have examined the combination of cinnamon and nutmeg that produces high hydrophobicity.(27) Although both are natural products, this paper utilized a organosilane-based alkyl and perfluorinated synthetic chemical coatings that raised some toxicity concerns due to high cuprous oxide content. We drew inspiration from the naturally occurring, extremely hydrophobic lotus leaves. These leaves expel water easily due to their micro-structural features, termed papillae, that exude epicuticular waxes, cutin.(28,29) Alternatively, Carnauba and beeswax have also high hydrophobicity that are routinely used in the food service industry.(30) With their high hydrophobicity, these solutions on food containers prevent waste by ensuring minimal food retention. However, there was a lack of clarity in the concentrations used in these prior formulations and the resulting hydrophobicity. The present study examined the different formulations of these two waxes together and evaluated the contact angle, sliding angle, and transmittance. The optimized formulation was subjected to durability testing with manual disinfectant procedures and long-term contact-wear testing.

MATERIALS AND METHODS

Formulation of anti-fogging solutions

Hydrophobic wax coatings were generated in acetone or methanol as solvents using ultrasonication. Different ratios of carnauba wax to beeswax (both Sigma Aldrich, St. Louis, MO) were employed namely 0.4375 g: 0.4375 g (1:1), 0.35 g: 0.525 g (1:1.5), 0.33 g: 0.66 g (1:2), 0.417 g: 0.834 g (1:2HC) were melted in a 50 ml plastic tube (Corning, Thermofisher Waltham, MA) in a water bath. After the waxes had melted, 25 milliliters of either acetone or methanol (both Sigma Aldrich, St. Louis, MO) were added, and the solution was emulsified immediately using a probe ultrasonication (Q2000, QSonica, Newtown CT) at 90% amplitude for 3 minutes and transferred into a 50 ml glass spray bottle.

Contact and Sliding Angle testing

Solutions were sprayed onto a 2 x 2-inch sheet of PETG at roughly a distance of 5 inches, spraying 10 times. After drying, the sheets of PETG were tested for contact angle, sliding angle, and transmission. A custom contact and sliding angle device were generated based on commercially available models using online CAD software (Onshape, PTC, Rockwell Automation, Boston MA). The devices were printed using Polylactic acid (PLA) filament (Overture, Overture 3D Technologies, Texas) on a i3 Prusa 3D printer (Prusa Research, Prague Czech Republic) (**Figs. 1 A - C**). The device included a slot for to hold a mobile phone to take digital pictures of the droplet. After fixing the plastic surface to the platform, droplets of water were generated with a 3 ml syringe and 14-gauge needle (to mimic humidity post-condensation on clear PPEs) and digital image were captured for analysis (**Fig. 1 D**). The digital images were analyzed using the NIH ImageJ (ver. 1.53n) software. The sliding angle set up included a protractor to assess the angle at which the droplet slides off. The platform was tilted slowly until the water droplet slid off, and the angle was documented (**Fig. 1 E**). All studies were performed in performed in triplicate and repeated atleast twice.

Transmittance analysis

The laser apparatus consisted of a 650 nm diode laser (Weber Medical, Beverungen, Germany) at 10 mW/cm^2, and a sensor with power meter (both Thor Labs, Newton NJ) (**Fig. 1F**). The sheets of PETG were placed on top of the power sensor, and transmission was assessed.

Optical clarity analysis

A sticker was placed on a bench and the sheets of PETG were placed over it. Digital pictures were taken with a mobile phone camera. The coated sheets of PETG were compared with the uncoated control and the visual clarity of the coatings was assessed.

Routine manual disinfection testing

The PETG coated surfaces were subjected to different solutions such as soap solution (10% v/v, Dawn, Procter & Gamble, Cincinnati OH), Isopropyl alcohol (70%, Sigma Aldrich, St. Louis MO), and water alone using paper towels (Uline, Milton ON), gauge (Henry Schein, New York, NY) or microfibers (Magic Fiber, Miami FL). These disinfectants were applied ten times in a uniform, lateral motion with manual pressure by a single operator. Disinfection wipes (Metrex, Orange CA) were used in another group.

Coating Durability following contact wear testing

To simulate accelerated contact wear testing, a custom apparatus was designed to mimic skin contact. Using the CAD software (Onshape, PTC, Rockwell Automation, Boston MA), a rotating platform with spring-loaded bases was designed to apply suitable skin contact forces. (31-33) The device was 3D printed with PLA filament (Overture, Overture 3D Technologies, Texas) on a i3 Prusa 3D printer (Prusa Research, Prague Czech Republic). The wheel was connected to a DC Motor (Greartisan, Shenzen Hotec, China) via a speed controller and a 9V battery which allowed the motor to function up to 1000 RPMs. After the coated samples were mounted on the platforms, the apparatus was positioned to allow the platforms to extend and retract using centrifugal force while spinning, hitting a skin-equivalent surface (rough side of oil-treated leather) to simulate contact. To simulate multiple skin contacts, the device was operated for 5 minutes, allowing each platform to contact the wall about 5000 times for each sample to simulate 4 weeks of routine wear. The contact force applied by the rotational, spring-loaded platform was measured with a digital force probe (Baoshishan, China). Following the contact wear testing, samples were assessed for changes in contact angle, sliding angle, transmittance and examined with topological analysis.

Topological analysis

Scanning electron microscopy (SEM) analysis was performed to determine the topology and the depth of the coating on the plastic sheet samples prior to and following wear testing. Samples were sputter-coated (Cressington 108, Ted Pella Inc, Redding CA) with carbon for 120 seconds and examined using SEM (Hitachi, S-4700, Japan) with a voltage of 2.0 kV at about 14.5$\pm$ 0.4 mm using secondary electron mode.

Statistical Analysis

Data was organized in Excel (Microsoft, Seattle WA) and presented as Means with standard deviations. Data was subjected to a Student's T test or two-way analysis of variance (ANOVA) among different treatments with Bonferroni's correction for multiple comparisons where appropriate. A $p < 0.05$ was considered statistically significant.

RESULTS

Formulation and Characterization of Anti-Fogging solutions

We first examined different ratios of carnauba and beeswax in two solvents namely Acetone and Ethanol to generate a homogenous solution (**Fig. 2A**). The contact angles of the acetone-based solutions were higher than their methanol counterparts (**Figs. 2B** and **2C**). The coating with the highest contact angle was the 1: 2 ratio in acetone solution with a mean contact angle of 150.3 $\pm$ 2.1 ^{o}. This categorizes this surface coating as highly hydrophobic compared to the other coatings and was significantly ($p < 0.05$) more hydrophobic than the uncoated plastic surface. We also examined the higher concentrations (HC) at 1 : 2 ratio to inquire if the density and hence, eventual coating concentration would affect these properties, but did not observe any further significantly improved characteristics. As expected the sliding angle for this coating was the lowest at 13.7 $\pm$ 2.1^{o} which was significantly ($p < 0.05$) lower than the uncoated plastic surface (**Figs. 2D** and **2E**). The transmittance of these formulation appears to vary with the concentration of the beeswax component as lower amounts resulted in higher transmittance (**Figs. 2F** and **2G**). The optical clarity was also assessed through the observation of the sticker through the coated slides. The optical clarity decreased as the concentrations of the solutes increased as was expected. The methanol-based formulations had a comparable degree of transmittance (0.41 to 0.33) than the acetone (0.3 to 0.26) counterparts compared to control (uncoated 0.43 $\pm$ 0.02). Based on these

results, we decided to pursue the 1:2 carnauba to bee wax in acetone formulation for subsequent studies.

Effect of routine disinfection procedures on durability of antifogging solution

The use of disinfectants is a necessary part of routine plastic mask and face shield use due to the prominent aerosol generating dental procedures. (34-36) Next, we examined routine disinfectant procedures employed in the dental office namely, soap, water, and 70% Isopropyl Alcohol with paper towels, gauze, or microfiber, and disinfectant wipes. We noted a significant ($p < 0.05$) reduction in the contact angle after all disinfection methods (**Fig. 3A**). Among all these methods, Isopropyl Alcohol with gauze reduced the contact angle the least (144.3 ± 1.6^{o}) while soap made the surface most hydrophilic (wettable), removing the coating most effectively. Concurrently, the sliding angle analysis showed a similar trend, increasing overall with all, but the soap group, disinfection methods (**Fig. 3B**). The Isopropyl alcohol group showed the least change and no statistically significant difference was noted when a paper towel was used. Interestingly, the transmittance appeared to vary after individual disinfectant methods with some showing increases while other showing significant decreases (**Fig. 3C**). The method of disinfection that showed most increase in light transmission were the sterilizing wipes by themselves. The lowest transmission was observed with Isopropyl Alcohol and soap with paper towels. Together, these results suggest that using Isopropyl Alcohol with gauze is optimal for disinfection as it minimally affects antifogging coating properties such as contact and sliding angle and transmission after repeated use.

Antifogging coating stability after contact wear testing

Finally, we investigated the durability of the anti-fogging solutions as they would be subjected to rigorous daily wear and tear during PPE use. We first created a simple rig to simulate skin contact based on a 3D printed apparatus (**Fig. 4A** and **B**). The rig was designed as a rotating platform that would result in a repetitive contact of the coated device with a stationary leather surface. The pressure exerted by facemask on the nose bridge and chin contact has been assessed to be 45 to 91 mm of Hg (6000-12,000 N/m^2) (**Fig. 4C**). (31-33) The constant skin contact force in our device was assessed to be 5000 N/m^2 that could be approximated to a repeated light skin contact.

Following the simulated wear, the contact and sliding angle as well as transmittance was assessed. We observed a significant reduction in contact angle (133.3 ± 1.5^{o}) and concomitant increase in the sliding angle (23.7 ± 1.5^{o}) compared to the uncoated control surfaces. While transmittance was not significantly different before and after wear simulation, there was a trend towards reduced transmission. Topological analysis noted the wear simulation resulted in significant accretions and scratches that likely contribute to the reduced light transmission observed. These results indicate that due to reduction in coating characteristics by about 50% over the simulated 4-week wear period, the coating will likely need to be replaced as often as every other week to maintain optimal functions.

DISCUSSION

The COVID pandemic presented new challenges to healthcare with an urgent need for innovations in disinfection approaches. The use of PPE was central in the attempts to mitigate the spread of infection and a major part of the solution to mitigate the health crisis. The use of these barriers continues to have an impact on both the psychological, and medical well-being of both the patients and the healthcare professionals themselves.(37) The initial response to the pandemic brought manufacturing and supply chain disruptions resulting in additive 3D printing enthusiasts to offer custom, local solutions. Our team at the University at Buffalo focused on the transparent PPE designs and dental loop attachments (**Fig. 5**). The condensation from breathing obscured the functions of the clear PPEs that presented a major impasse to their use. This work was specifically motivated to address this deterrent to routine clear PPE use.

We tested polyethylene terephthalate glycol (PETG). PETG is a commonly-used thermoplastic with impact resistance, durability, ductility, chemical resistance properties well-suited to this application. To generate an anti-fogging solution for our clear face shields and masks, a major design challenge was the close proximity to nose and mouth.(38,39) We chose to pursue natural waxes as the main ingredient as they provided a natural, non-toxic solution that has a well-established track record of biological safety. (40) The other major component constituent was a polar solvent to enhance miscibility and dispersion of these waxes. We chose to examine Acetone and Ethanol in our formulation. The acetone formulation was superior in generating the most hydrophobic product after spray coating. Our initial efforts at dissolving the waxes in Acetone

(boiling point of 55.5°C) by heating alone resulted in evaporation and non-uniform dissolution. Hence, we chose to disperse the waxes via ultrasonication. Among the various formulations, the most hydrophobic surface was generated by the 1 : 2 ratio (contact angle 150.3 $\pm$ 2.1°) though the other formulations were also strongly hydrophobic (contact angles 121 to 135°). We also examined Methanol (boiling point of 148.5 °F) in the same volume that, in contrast, generated hydrophilic surface coatings with all formulations (contact angles 34 to 82 °), but most prominently with the 1 : 2 at the higher concentration (contact angle 80.7 $\pm$ 2.1 °). Increasing the concentration in the Methanol formulation (1 : 2 HC) appeared to impact the physical characteristics more than the Acetone (1 : 2 HC) formulation that could eb attributed to differential dissolution of the waxes and subsequent homogeneity of the coating film. Among the two solvents examined, Methanol did not enable a suitable anti-fogging formulation and hence, the 1: 2 formulation in Acetone was chosen as an optimal anti-fogging solution. This may have been due to the fact that methanol has a higher polarity than acetone that facilitates improved dispersibility of the non-polar wax compounds.

The use of surface disinfectants is an integral part of maintaining and reusing PPEs. This is a sustainable and cost-effective practice that is routinely employed. A key design requirement of the anti-fogging solution is durability with these disinfectant approaches. We observed that the soap solution group consistently demonstrated complete removal of the anti-fogging solution. While this desirable as a disinfectant approach to remove all potentially hazardous aerosols on these PPEs, its amphiphilic nature allowing it to form micelles with the wax components of the anti-fogging solution would deem it unsuitable. The removal of the anti-fogging solution with these approaches could be attributed to the surfactant nature that interferes with the surface tension of the water droplets. Another possibility is that the lipid-to-lipid interaction of the soap and the waxes may inactivate the hydrophobic nature of the coating. The superior solubilizing ability of isopropyl alcohol that may further smoothen the coating, reduce surface tension further or alter drying times are areas of future investigations.

To investigate the durability of the anti-fogging coating, we generated a custom rig for accelerated surface contact testing. The major design principle for this device was to generate a PPE skin contact force. The reported PPE skin contact force to create a tight seal on the nose and chin has been reported as 45 to 91 mm of Hg (6000-12,000 N/m^2). (31-33) The force generated by our rig was lower at 5000 N/m^2 and was intended to approximate light skin contact force in non-

fastened areas. This reflects routine surface contact during routine use of the PPEs. The hydrophobicity of the anti-fogging surfaces was relatively well maintained (contact angle 133.3 $\pm$ 1.5^{o} and sliding angle 23.7 $\pm$ 1.5^{o}). However, the durability testing noted a reduction in the transmittance of the masks that could be attributed the wear from the contact forces. As evident in the ultrastructural analysis, the PETG surface appears to have several accretions and disruption of the uniform coated surfaces. Given these PPEs are disposable and have a limited time of use, this may not significantly impact the PPE performance. In fact, this lack of clarity from routine use may be a good marker for replacement with a simple optical interferometry device.

This study has a few limitations. First, the biological performance of this anti-fogging solution could be examined using *in vitro* (reconstructed human epidermis), and *in vivo* skin contact testing in animals and human studies. (41-47) While this could be considered routine diligence, it is prudent to emphasize both the waxes and PETG are generally regarded as safe (FDA GRAS) and are used in current product (e.g; lip balm) formulations routinely. The solvents are readily eliminated by mild heating (40 ^{o}C overnight). Second, applying a hydrophobic solution on the PETG clear surface may, counter to its primary objective, worsen the visibility due to the moisture coalescing into larger water beads. It is conceivable that the increasing size of these water beads may eventually reach a critical mass and cause them to slide off. This phenomenon is observed on hydrophobic surfaces like lotus leaves and commercial car wax coatings. Hence, a replaceable absorbent liner and a mild, mechanical vibration module to promote water droplet beading and run-off could be attractive future design iteration in these clear PPEs. Third, a major shortcoming of using such an anti-fogging spray is its temporary nature and the need for continuous replacement throughout the lifetime of the clear PPE. Thus, a potential future possibility is to pursue nanopatterning, simulating the lotus leaf papillae for a more biocompatible, permanent anti-fogging solution.

Conclusions

In summary, this work demonstrates the utility of an anti-fogging formulation with two natural waxes that has good durability and optimal non-fouling properties. This solution represents a cost-effective, durable, non-toxic approach to prevent or reduce fogging of clear PPEs such as plastic masks and face shields from condensations of humidity arising from breathing and speaking.

Conflicts of Interests

The authors declare they have no relevant conflicts of interest with this work.

Acknowledgements

We thank the members of the Buffalo3DPPE for their time and effort during the pandemic namely, Kierra Bleyle, Preethi Singh, Jason Ciano, Savannah Tomaka, Jacob Graca, Hunter Rosa, Yianni Savidis, Danielle Detwiler, Omer Hillel, and Georgia Kyriacou. We also thank the Buffalo Enable (BE Mask) team for their valuable collaboration and technical assistance with 3D printing namely Aaron Gorsline, Albert Titus, James Whitlock, Peter Elkin, Jeremy Simon, Jon Schull, Ben Rubin, Kelly Cheatle, Pete Suffoletto, and Skip Meetze. We would like to thank Mr. Peter Bush, South Campus Instrument core for assisting with the SEM analysis and Weber Medical laser for providing their laser device. This work was supported by the BlueSky, University at Buffalo, and Dean's fund, School of Dental Medicine.

References

1. Pak A, Adegboye OA, Adekunle AI, Rahman KM, McBryde ES, Eisen DP. Economic Consequences of the COVID-19 Outbreak: the Need for Epidemic Preparedness. Front Public Health 2020; 8:241.
2. Pirasteh-Anosheh H, Parnian A, Spasiano D, Race M, Ashraf M. Haloculture: A system to mitigate the negative impacts of pandemics on the environment, society and economy, emphasizing COVID-19. Environ Res 2021; 198:111228.
3. Goriuc A, Sandu D, Tatarciuc M, Luchian I. The Impact of the COVID-19 Pandemic on Dentistry and Dental Education: A Narrative Review. Int J Environ Res Public Health 2022; 19(5).
4. Kurian N, Gandhi S, Thomas AM. COVID-19 and multidisciplinary dentistry. Br Dent J 2021; 231(9):534.
5. Lieberthal B, McCauley LK, Feldman CA, Fine DH. COVID-19 and Dentistry: Biological Considerations, Testing Strategies, Issues, and Regulations. Compend Contin Educ Dent 2021; 42(6):290-296; quiz 297.
6. Artenstein AW. In Pursuit of PPE. N Engl J Med 2020; 382(18):e46.
7. Marcus K, Balasubramanian M, Short SD, Sohn W. Dental hesitancy: a qualitative study of culturally and linguistically diverse mothers. BMC Public Health 2022; 22(1):2199.
8. Muneer MU, Ismail F, Munir N, Shakoor A, Das G, Ahmed AR, Ahmed MA. Dental Anxiety and Influencing Factors in Adults. Healthcare (Basel) 2022; 10(12).
9. Nikolic M, Mitic A, Petrovic J, Dimitrijevic D, Popovic J, Barac R, Todorovic A. COVID-19: Another Cause of Dental Anxiety? Med Sci Monit 2022; 28:e936535.
10. Blais C, Fiset D, Roy C, Saumure Regimbald C, Gosselin F. Eye fixation patterns for categorizing static and dynamic facial expressions. Emotion 2017; 17(7):1107-1119.
11. Chodosh J, Weinstein BE, Blustein J. Face masks can be devastating for people with hearing loss. BMJ 2020; 370:m2683.

12. Chu JN, Collins JE, Chen TT, Chai PR, Dadabhoy F, Byrne JD, Wentworth A, DeAndrea-Lazarus IA, Moreland CJ, Wilson JAB, Booth A, Ghenand O, Hur C, Traverso G. Patient and Health Care Worker Perceptions of Communication and Ability to Identify Emotion When Wearing Standard and Transparent Masks. JAMA Netw Open 2021; 4(11):e2135386.
13. Fleming JT, Maddox RK, Shinn-Cunningham BG. Spatial alignment between faces and voices improves selective attention to audio-visual speech. J Acoust Soc Am 2021; 150(4):3085.
14. MacLeod A, Summerfield Q. Quantifying the contribution of vision to speech perception in noise. Br J Audiol 1987; 21(2):131-141.
15. Schwartz JL, Berthommier F, Savariaux C. Seeing to hear better: evidence for early audio-visual interactions in speech identification. Cognition 2004; 93(2):B69-78.
16. Sonnichsen R, Llorach To G, Hochmuth S, Hohmann V, Radeloff A. How Face Masks Interfere With Speech Understanding of Normal-Hearing Individuals: Vision Makes the Difference. Otol Neurotol 2022; 43(3):282-288.
17. Atcherson SR, Mendel LL, Baltimore WJ, Patro C, Lee S, Pousson M, Spann MJ. The Effect of Conventional and Transparent Surgical Masks on Speech Understanding in Individuals with and without Hearing Loss. J Am Acad Audiol 2017; 28(1):58-67.
18. Belhouideg S. Impact of 3D printed medical equipment on the management of the Covid19 pandemic. Int J Health Plann Manage 2020; 35(5):1014-1022.
19. O'Connor S, Mathew S, Dave F, Tormey D, Parsons U, Gavin M, Nama PM, Moran R, Rooney M, McMorrow R, Bartlett J, Pillai SC. COVID-19: Rapid prototyping and production of face shields via flat, laser-cut, and 3D-printed models. Results Eng 2022; 14:100452.
20. Rupesh Kumar J, Mayandi K, Joe Patrick Gnanaraj S, Chandrasekar K, Sethu Ramalingam P. A critical review of an additive manufacturing role in Covid-19 epidemic. Mater Today Proc 2022; 68:1521-1527.
21. Vallatos A, Maguire JM, Pilavakis N, Cerniauskas G, Sturtivant A, Speakman AJ, Gourlay S, Inglis S, McCall G, Davie A, Boyd M, Tavares AAS, Doherty C, Roberts S, Aitken P, Mason M, Cummings S, Mullen A, Paterson G, Proudfoot M, Brady S, Kesterton S, Queen F, Fletcher S, Sherlock A, Dunn KE. Adaptive Manufacturing for Healthcare During the COVID-19 Emergency and Beyond. Front Med Technol 2021; 3:702526.
22. Kalkal A, Allawadhi P, Kumar P, Sehgal A, Verma A, Pawar K, Pradhan R, Paital B, Packirisamy G. Sensing and 3D printing technologies in personalized healthcare for the management of health crises including the COVID-19 outbreak. Sens Int 2022; 3:100180.
23. Arany PSaP. Dental Faceshields. 2020.
24. Wahab IF, Bushroa AR, Teck SW, Azmi TT, Ibrahim MZ, Lee JW. Fundamentals of antifogging strategies, coating techniques and properties of inorganic materials; a comprehensive review. Journal of Materials Research and Technology 2023; 23.
25. Laurén S. Contact angle measurements on superhydrophobic surfaces in practice. Surface Science Blog: Biolin Scientific; 2019.
26. Lv C, Yang C, Hao P, He F, Zheng Q. Sliding of water droplets on microstructured hydrophobic surfaces. Langmuir 2010; 26(11):8704-8708.
27. Razavi SMR OJ, Sett S, et al. Superhydrophobic Surfaces Made from Naturally Derived Hydrophobic Materials. ACS Sustainable Chem Eng 2016.
28. Bormashenko E. Wetting of real solid surfaces: new glance on well-known problems. Colloid and Polymer Science 2013.
29. Li P. Submillimeter Papillae: Shape Control of Lotus Leaf Induced by Surface Submillimeter Texture. Advanced Materials Interfaces 2020.
30. Wang P QX, Shen J. Superhydrophobic Coatings with Edible Biowaxes for Reducing or Eliminating Liquid Residues of Foods and Drinks in Containers. Bioresources 2018.

31. Brill AK, Pickersgill R, Moghal M, Morrell MJ, Simonds AK. Mask pressure effects on the nasal bridge during short-term noninvasive ventilation. ERJ Open Res 2018; 4(2).
32. Dellweg D, Hochrainer D, Klauke M, Kerl J, Eiger G, Kohler D. Determinants of skin contact pressure formation during non-invasive ventilation. J Biomech 2010; 43(4):652-657.
33. Schettino GP, Tucci MR, Sousa R, Valente Barbas CS, Passos Amato MB, Carvalho CR. Mask mechanics and leak dynamics during noninvasive pressure support ventilation: a bench study. Intensive Care Med 2001; 27(12):1887-1891.
34. Epstein JB, Chow K, Mathias R. Dental procedure aerosols and COVID-19. Lancet Infect Dis 2021; 21(4):e73.
35. Mick P, Murphy R. Aerosol-generating otolaryngology procedures and the need for enhanced PPE during the COVID-19 pandemic: a literature review. J Otolaryngol Head Neck Surg 2020; 49(1):29.
36. Wilson NM, Norton A, Young FP, Collins DW. Airborne transmission of severe acute respiratory syndrome coronavirus-2 to healthcare workers: a narrative review. Anaesthesia 2020; 75(8):1086-1095.
37. Kisielinski K, Giboni P, Prescher A, Klosterhalfen B, Graessel D, Funken S, Kempski O, Hirsch O. Is a Mask That Covers the Mouth and Nose Free from Undesirable Side Effects in Everyday Use and Free of Potential Hazards? Int J Environ Res Public Health 2021; 18(8).
38. Rothe H, Fautz R, Gerber E, Neumann L, Rettinger K, Schuh W, Gronewold C. Special aspects of cosmetic spray safety evaluations: principles on inhalation risk assessment. Toxicol Lett 2011; 205(2):97-104.
39. Tha EL, Canavez A, Schuck DC, Gagosian VSC, Lorencini M, Leme DM. Beyond dermal exposure: The respiratory tract as a target organ in hazard assessments of cosmetic ingredients. Regul Toxicol Pharmacol 2021; 124:104976.
40. Final Report on the Safety Assessment of Candelilla Wax, Carnauba Wax, Japan Wax, and Beeswax. J Am Coll Toxicol 1984; 3(3).
41. Arnesdotter E, Rogiers V, Vanhaecke T, Vinken M. An overview of current practices for regulatory risk assessment with lessons learnt from cosmetics in the European Union. Crit Rev Toxicol 2021; 51(5):395-417.
42. Choksi NY, Truax J, Layton A, Matheson J, Mattie D, Varney T, Tao J, Yozzo K, McDougal AJ, Merrill J, Lowther D, Barroso J, Linke B, Casey W, Allen D. United States regulatory requirements for skin and eye irritation testing. Cutan Ocul Toxicol 2019; 38(2):141-155.
43. Filaire E, Nachat-Kappes R, Laporte C, Harmand MF, Simon M, Poinsot C. Alternative in vitro models used in the main safety tests of cosmetic products and new challenges. Int J Cosmet Sci 2022; 44(6):604-613.
44. Hardwick RN, Betts CJ, Whritenour J, Sura R, Thamsen M, Kaufman EH, Fabre K. Drug-induced skin toxicity: gaps in preclinical testing cascade as opportunities for complex in vitro models and assays. Lab Chip 2020; 20(2):199-214.
45. Nabarretti BH, Rigon RB, Burga-Sanchez J, Leonardi GR. A review of alternative methods to the use of animals in safety evaluation of cosmetics. Einstein (Sao Paulo) 2022; 20:eRB5578.
46. Pistollato F, Madia F, Corvi R, Munn S, Grignard E, Paini A, Worth A, Bal-Price A, Prieto P, Casati S, Berggren E, Bopp SK, Zuang V. Current EU regulatory requirements for the assessment of chemicals and cosmetic products: challenges and opportunities for introducing new approach methodologies. Arch Toxicol 2021; 95(6):1867-1897.
47. Riebeling C, Luch A, Tralau T. Skin toxicology and 3Rs-Current challenges for public health protection. Exp Dermatol 2018; 27(5):526-536.

441

442

443

444

Figure Legends

Figure 1. Physical characterization of anti-fogging coating

(**A.**) CAD of the contact angle apparatus for 3D printing (**B.**) CAD of the sliding angle module for 3D printing (**C.**) 3D printed models of contact and sliding angle testing apparatus (**D.**) Image of the contact angle assessment showing droplet generation and analysis. Inset shows the digital analysis of contact angle ϕ using NIH ImageJ (**E.**) Digital image analysis showing the sliding angle measurement using NIH ImageJ (**F.**) transmittance set-up using a diode laser and optical power meter with the sensor.

Figure 2. Anti-fogging solution formulation and characterization

(A.) Tabular outline of the formulation depicting ratios of carnauba and beeswax in acetone and methanol used to coat PETG plastic sheets (**B.** and **C.**) Contact angle assessment of Acetone and Methanol formulations at various concentrations (**D** and **E**) Sliding angle analysis of Acetone and Methanol formulations at various concentrations (**F** and **G**) Transmission of diode laser for transmittance assessment of Acetone and Methanol formulations at various concentrations. (**I.**) Digital image of an uncoated, Acetone and Methanol formulations applied to the PETG sheet. Data are shown as Mean and SD and representative of at least two independent studies. Statistical significance was determined using two-way analysis of variance (ANOVA) among different treatments using Bonferroni's multiple comparison test (n = 3). Statistical significance is denoted as * $p < 0.05$, ** $p < 0.005$, and *** $p < 0.0005$.

Figure 3. Effects of Disinfection on anti-fogging coating integrity

(**A.**) Contact angle assessment after various disinfection procedures (**B.**) Sliding angle analysis after various disinfection procedures (**C.**) transmittance after various disinfection procedures. Data are shown as Mean and SD and representative of at least two independent studies. Statistical

468 significance was determined using two-way analysis of variance (ANOVA) among different
469 treatments using Bonferroni's multiple comparison test (n = 3). Statistical significance is denoted
470 as * $p < 0.05$, ** $p < 0.005$, *** $p < 0.0005$, and **** $p < 0.00005$.

471

472

473 **Figure 4. Durability testing of anti-fogging coating following contact testing**

474 (**A.**) CAD of contact testing apparatus used for wear testing analysis (**B**.) 3D printed model of the
475 assembled contact testing apparatus (**C.**) Outline of the eminent forces determining the contact
476 force on PETG surfaces. The contact angle (**D.**), sliding angle (**E.**), and transmittance (**F**.) analysis
477 before and after contact testing (**G.**) Scanning electron microscopy images of the uncoated and
478 coated surfaces before and after contact testing. Data are shown as Mean and SD and representative
479 of at least two independent studies. Statistical significance was determined using the Students' T-
480 test (n = 3). Statistical significance is denoted as * $p < 0.05$.

481

482 **Figure 5. Clear face shields and masks**

483 A clear mask design with filter unit in medium (**A.**) and large (**B.**) sizes. The 3D printed clear face
484 shields are shown to accommodate different dental operating loupes such as Eclipse (**C.**), Vision,
485 Surgitel and Orascoptic (**D.**). Images are provided with consent from lab volunteers from the
486 website www.buffalo3dppe.com.

Figure 1

Figure 1. Physical characterization of anti-fogging coating

(**A.**) CAD of the contact angle apparatus for 3D printing (**B.**) CAD of the sliding angle module for 3D printing (**C.**) 3D printed models of contact and sliding angle testing apparatus (**D.**) Image of the contact angle assessment showing droplet generation and analysis. Inset shows the digital analysis of contact angle φ using NIH ImageJ (**E.**) Digital image analysis showing the sliding angle measurement using NIH ImageJ (**F.**) transmittance set-up using a diode laser and optical power meter with the sensor.

Fig. 1

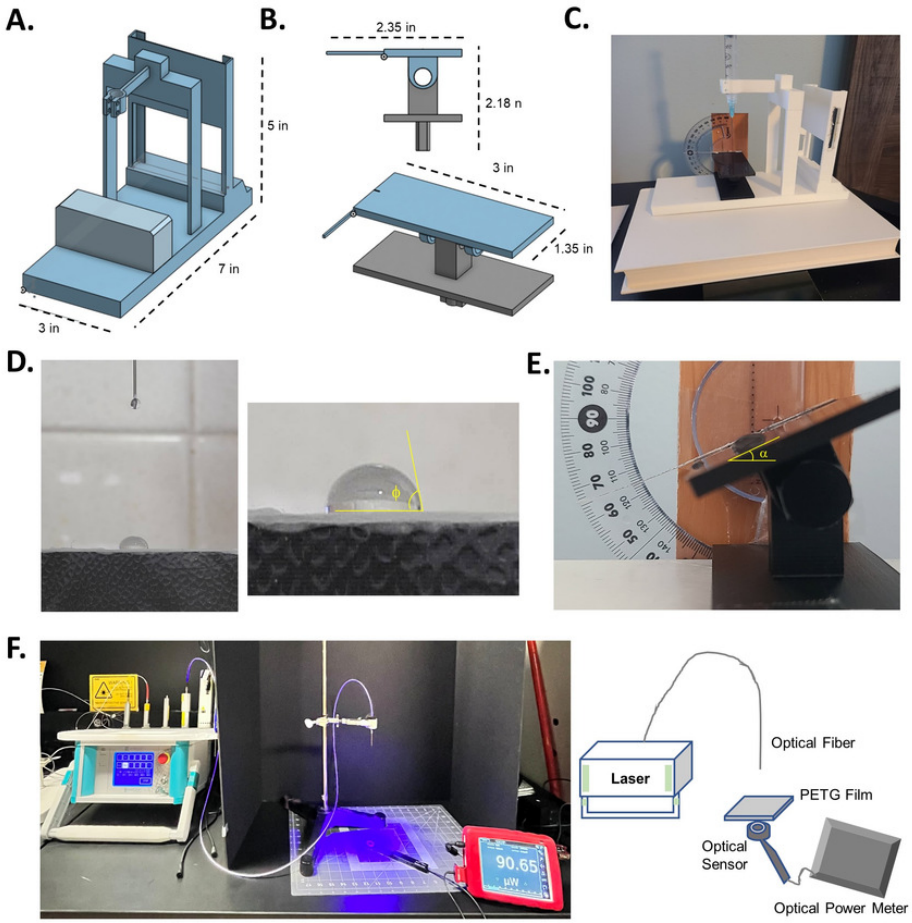
A.
5 in
7 in
3 in
B.
2.35 in
2.18 n
3 in
1.35 in
C.
D.
E.
F.
Laser
Optical Fiber
PETG Film
Optical Sensor
Optical Power Meter
90.65
μW

Figure 2

Figure 2. Anti-fogging solution formulation and characterization

<!--[if !supportLists]-->**(A.)** <!--[endif]-->Tabular outline of the formulation depicting ratios of carnauba and beeswax in acetone and methanol used to coat PETG plastic sheets (**B.** and **C.**) Contact angle assessment of Acetone and Methanol formulations at various concentrations (**D** and **E**) Sliding angle analysis of Acetone and Methanol formulations at various concentrations (**F** and **G**) Transmission of diode laser for transmittance assessment of Acetone and Methanol formulations at various concentrations. (**I.**) Digital image of an uncoated, Acetone and Methanol formulations applied to the PETG sheet. Data are shown as Mean and SD and representative of at least two independent studies. Statistical significance was determined using two-way analysis of variance (ANOVA) among different treatments using Bonferroni's multiple comparison test (n = 3). Statistical significance is denoted as * $p < 0.05$, ** $p< 0.005$, and *** $p< 0.0005$.

Fig. 2

A.

Ratio	Carnauba (g)	Beeswax (g)	Acetone/Methanol (ml)
1:1	0.4375	0.4375	25
1:1.5	0.35	0.525	25
1:2	0.33	0.67	25
1:2 (HC)	0.417	0.833	25

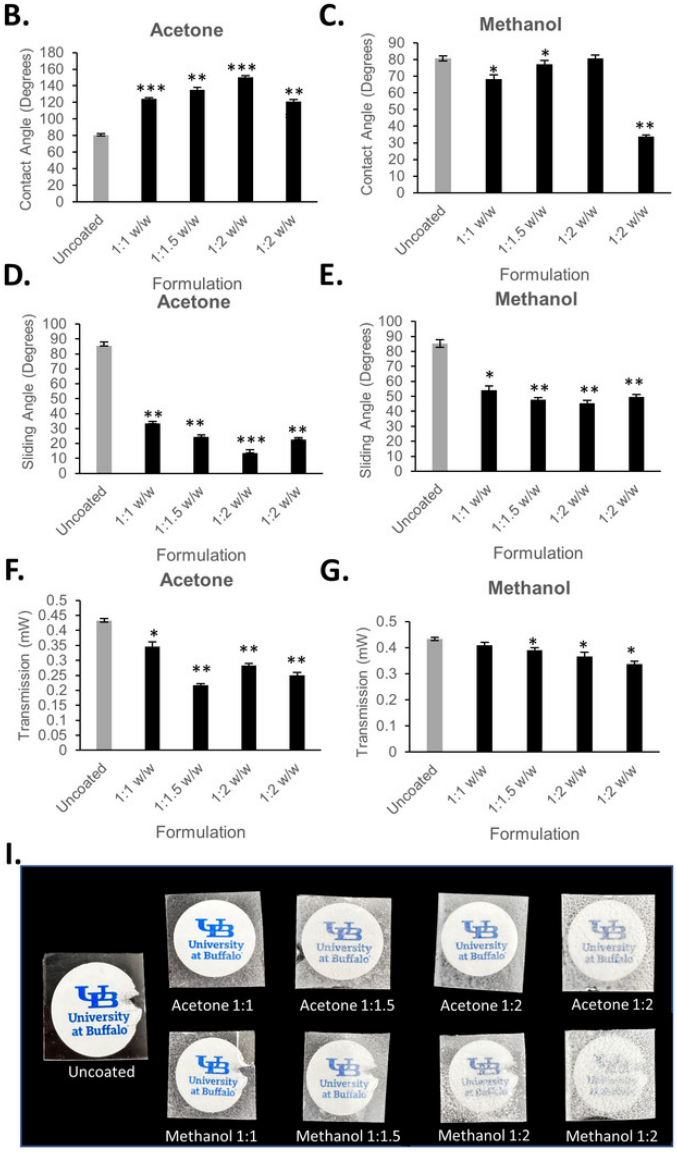

Figure 3

Figure 3. Effects of Disinfection on anti-fogging coating integrity

(**A.**) Contact angle assessment after various disinfection procedures (**B.**) Sliding angle analysis after various disinfection procedures (**C.**) transmittance after various disinfection procedures. Data are shown as Mean and SD and representative of at least two independent studies. Statistical significance was determined using two-way analysis of variance (ANOVA) among different treatments using Bonferroni's multiple comparison test (n = 3). Statistical significance is denoted as * $p < 0.05$, ** $p < 0.005$, *** $p < 0.0005$, and **** $p < 0.00005$.

Fig. 3

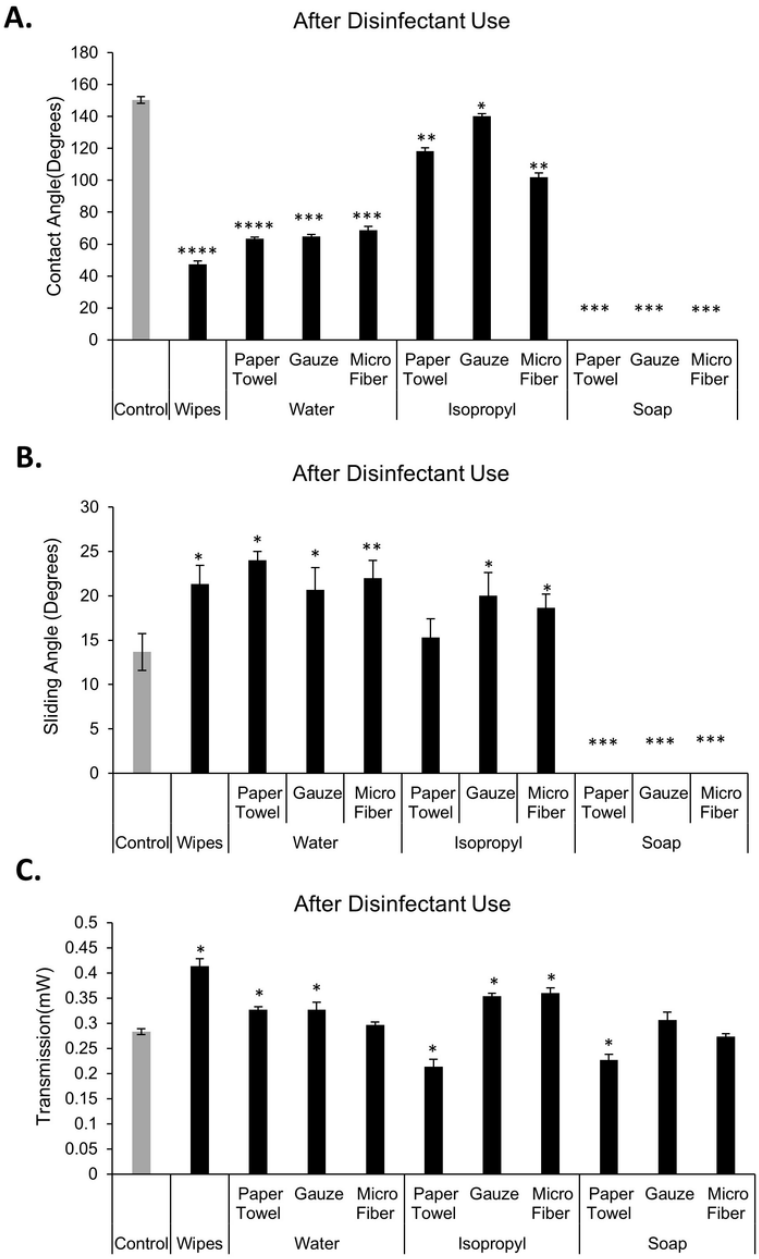
A.
After Disinfectant Use
Contact Angle(Degrees)
180
160
140
120
100
80
60
40
20
0
Control
Wipes
Paper Towel
Gauze
Micro Fiber
Water
Isopropyl
Soap
B.
After Disinfectant Use
Sliding Angle (Degrees)
30
25
20
15
10
5
0
C.
After Disinfectant Use
Transmission(mW)
0.5
0.45
0.4
0.35
0.3
0.25
0.2
0.15
0.1
0.05
0

Figure 4

Figure 4. Durability testing of anti-fogging coating following contact testing

(**A.**) CAD of contact testing apparatus used for wear testing analysis (**B**.) 3D printed model of the assembled contact testing apparatus (**C.**) Outline of the eminent forces determining the contact force on PETG surfaces. The contact angle (**D.**), sliding angle (**E.**), and transmittance (**F**.) analysis before and after contact testing (**G.**) Scanning electron microscopy images of the uncoated and coated surfaces before and after contact testing. Data are shown as Mean and SD and representative of at least two independent studies. Statistical significance was determined using the Students' T-test (n = 3). Statistical significance is denoted as * $p < 0.05$.

Fig. 4

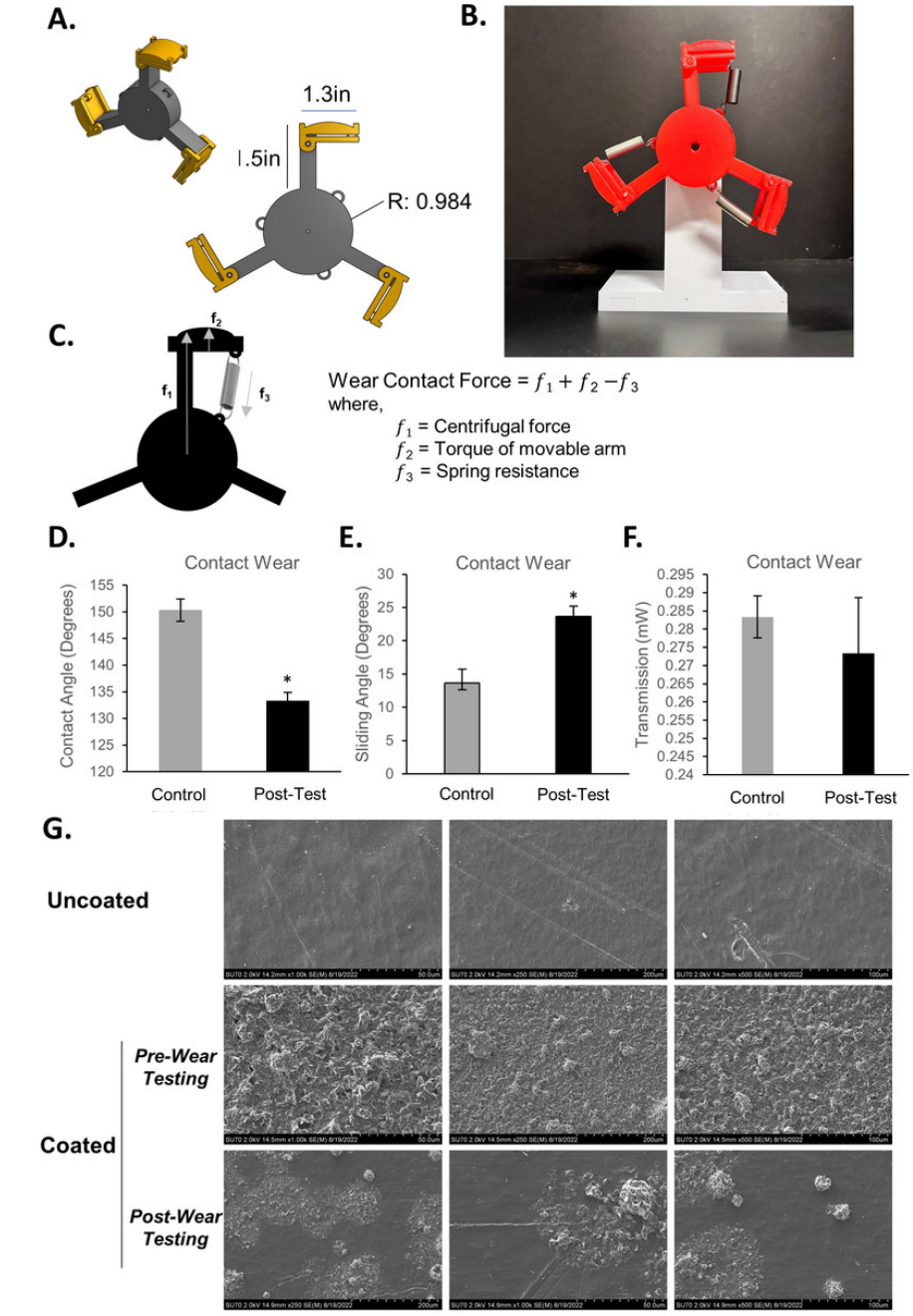
A.
1.3in
1.5in
R: 0.984
B.
C.
f2
f1
f3
Wear Contact Force = $f_1 + f_2 - f_3$
where,
f_1 = Centrifugal force
f_2 = Torque of movable arm
f_3 = Spring resistance
D.
Contact Wear
Contact Angle (Degrees)
155
150
145
140
135
130
125
120
Control
Post-Test
E.
Contact Wear
Sliding Angle (Degrees)
30
25
20
15
10
5
0
Control
Post-Test
F.
Contact Wear
Transmission (mW)
0.295
0.29
0.285
0.28
0.275
0.27
0.265
0.26
0.255
0.25
0.245
0.24
Control
Post-Test
G.
Uncoated
Coated
Pre-Wear Testing
Post-Wear Testing

Figure 5

Figure 5. Clear face shields and masks

A clear mask design with filter unit in medium (**A.**) and large (**B.**) sizes. The 3D printed clear face shields are shown to accommodate different dental operating loupes such as Eclipse (**C.**), Vision, Surgitel and Orascoptic (**D.**). Images are provided with consent from lab volunteers from the website www.buffalo3dppe.com .

Fig. 5